

System Identification Guidance For Multirotor Aircraft: Dynamic Scaling and Test Techniques

Christina M. Ivler
Assistant Professor
University of Portland
Portland, OR, U.S.

Elizabeth S. Rowe
Mechanical Engineering
Student
University of Portland
Portland, OR, U.S.

James Martin
Mechanical Engineering
Student
University of Portland
Portland, OR, U.S.

Mark J. S. Lopez
Aerospace Engineer
Aviation Development Directorate
U.S. Army CCDC, AvMC
Moffett Field, CA, U.S.

Mark B. Tischler, ST
Senior Scientist
Aviation Development Directorate
U.S. Army CCDC, AvMC
Moffett Field, CA, U.S.

ABSTRACT

State-space system identification was performed in order to extract flight dynamic models for hovering flight of a 56 cm, 1.56 kg hexacopter unmanned aerial vehicle (UAV). Different input excitation techniques were tested to determine which maneuvers provided high quality system identification results for small scale multirotor vehicles. These input excitation techniques included automated frequency sweeps, varying in amplitude, and multi-sine sweeps. Coherence, Cramer-Rao bounds, and insensitivities were used as metrics for comparing the system identification results. A parametric variation of frequency sweep amplitudes were performed in all axes (roll, yaw, pitch and heave) in order to provide guidance on frequency sweep amplitude for small scale multirotor unmanned aerial systems (UAS). The dynamics of the 56 cm hexacopter were used to estimate the dynamics of a larger 127 cm hexacopter via Froude scaling based on hub-to-hub distance as the characteristic length. The scaled results were compared to an actual system identification model of a 127 cm hexacopter.

NOMENCLATURE

p, q, r = body axis roll, pitch and yaw rates
 ϕ, θ, ψ = body axis pitch, roll, and yaw attitudes
 a_x, a_y, a_z = body axis accelerometer measurements
 u, v, w = body axis velocities, m/s
 T = Motor lag states
 δ = control deflection, $\frac{\%}{100}$
 λ_i = i^{th} eigenvalue of identified model, rad/s
 J = model validation cost function

Subscripts

lon = longitudinal (pitch) control input
lat = lateral (roll) control input
yaw = yaw control input
thr = throttle (heave) control input

Acronyms

UAV = Unmanned Aerial Vehicle
UAS = Unmanned Aerial Systems
CIFER = Comprehensive Identification from
Frequency Responses
GCS = Ground Control Station

INTRODUCTION

Unmanned aerial vehicles (UAVs) are serving as a new way to perform autonomous tasks [1]. Multirotor aerial vehicles are emerging as a popular configuration because of their mechanical simplicity and vertical lift capability [2]. Developing accurate flight dynamic models of these aircraft is an important step to simulate and predict the behavior of a UAV. Flight accurate computer simulations allow engineers to test the design and control systems in desktop and hardware in the loop simulations [3], ultimately abating flight time and cost. System identification is a rapid method for extracting dynamic models from

flight test data. A small scale hexacopter (1.56 kg, 56 cm diameter) operated by the University of Portland was used to study system identification of small-scale multirotor UAVs using CIFER® [4]. Although frequency domain system identification has been previously applied to quadrotors [2, 3] this was one of the first applications to a hexacopter. As unique unmanned aerial vehicle configurations increase in popularity, physical models are not well validated; as such, flight accurate system identification models are taking a larger role. Although system identification flight test methods for large-scale manned vehicles are well documented [4], guidance on flight test methods for system identification of small scale multirotor unmanned aerial vehicles are not as readily available.

A key aspect of the frequency domain system identification procedure is performing maneuvers to excite the aircraft across the frequency range of interest for system identification. Frequency sweeps are popular flight maneuvers to gather data about the vehicle dynamics as these inputs provide a rich spectral excitation [4]. Published research papers involving system identification of small-scale vehicles state that the UAV was excited using frequency sweep maneuvers, however, did not go into detail about how the frequency sweeps inputs were designed (in terms of duration, magnitude, frequency range, etc.) [3, 5]. Additionally, multi-sine maneuvers are another way to collect flight data in order to perform frequency domain system identification [6, 7]. There is a need for guidance in techniques used for gathering flight test data for small scale unmanned aerial vehicles in order to produce high quality system identification results with minimal trial and error.

In addition to understanding how the system identification methods scale with size of the vehicle, it was also of interest to understand the scaling of the dynamics of multirotor vehicles as they grow or shrink in size. Looking toward development of flying/handling qualities specifications for unmanned systems, as in Refs. [8, 9, 10, 11, 12], a critical first step is to determine the methods for scaling common configurations with size, so that the handling qualities specifications can also be scaled accordingly. The ultimate goal, although outside the scope of this paper, is to provide a generic framework for scaling handling qualities specifications for any class of multirotor vehicle. This will ensure that requirements developed for one multirotor aircraft can be scaled and used as a generic guidance for that size of vehicle, as opposed to developing new specifications for every possible multirotor UAS.

BACKGROUND

Flight Vehicle

A custom hexacopter built at the University of Portland (UP) was used to study system identification of small scale UAVs. The UP hexacopter weighs 1.56 kg with the 4S battery and is 56 cm in diameter (hub-to-hub). The hexacopter was built using a DJI Flame-wheel F550 frame, 930 kV motors, 30A electronic speed controllers and 10-inch diameter rotors. The hexacopter as configured for flight is shown in *Figure 1*.

ArduPilot is an open-source software suite that bundles together sensor processing, flight control, and navigation software [1]. A branch of the ArduPilot software is ArduCopter that supports a variety of multirotor configurations such as quadcopter, hexacopter, and octocopter configurations. The autopilot controller board, Pixhawk Mini (*Figure 2*), was chosen for the UP hexacopter due to its general application, reduced size, reliable navigation and improved sensors [1]



Figure 1. University of Portland Hexacopter.



Figure 2. Pixhawk Mini Autopilot Controller Board.

The UP hexacopter also shares information with a ground control station (GCS) using a wireless 3DR 915MHz telemetry radio [1]. The ground control station, Mission Planner, was utilized to show real-time data on the UAV's position, upload commands, and set parameters. Mission Planner was also used to analyze downloaded missions, and use telemetry to monitor, record, and view mission logs [1].

A tethering system was developed in order to ensure that the hexacopter would not depart from the testing area. The tether was designed to avoid interference with the dynamics of the hexacopter. Light-weight survival Kevlar cord (rated to 200 lb) was tied to each leg of the hexacopter and to a thirty-pound kettle bell with double figure eight knots used to secure the cord to each arm. Two lightweight aluminum rings were attached to segments part way down the cord in order to weigh the Kevlar cord down enough so that it did not lift and interfere with the blades of the hexacopter during flight but was light enough that it did not effect the dynamics of the vehicle. A bungee cord with a carabiner was attached to the kettle bell and cord in order to prevent sudden tugging of the cord when the hexacopter is out of range. The cord was limited to 35 feet based on the dimensions of the testing area.

$$\begin{bmatrix} \dot{v} \\ \dot{p} \\ \dot{r} \\ \dot{\phi} \\ \dot{T}_{lat} \\ \dot{T}_{yaw} \end{bmatrix} = \begin{bmatrix} Y_v & 0 & 0 & -g & 0 & 0 \\ L_v & L_p & 0 & 0 & L_{\delta_{lat}} & 0 \\ 0 & 0 & N_r & 0 & 0 & N_{\delta_{yaw}} \\ 0 & 1 & 0 & 0 & 0 & 0 \\ 0 & 0 & 0 & 0 & -\omega_{lag} & 0 \\ 0 & 0 & 0 & 0 & 0 & -\omega_{lag} \end{bmatrix} \begin{bmatrix} v \\ p \\ r \\ \phi \\ T_{lat} \\ T_{yaw} \end{bmatrix} + \begin{bmatrix} 0 & 0 \\ 0 & 0 \\ 0 & N'_{\delta_{yaw}} \\ 0 & 0 \\ \omega_{lag} & 0 \\ 0 & \omega_{lag} \end{bmatrix} \begin{bmatrix} \delta_{lat}(t - \tau) \\ \delta_{yaw}(t - \tau) \end{bmatrix} \quad (1)$$

The inputs to the model are the lateral control axis input δ_{lat} and the yaw control axis input δ_{yaw} , both measured just upstream of the mixer (in normalized units, %/100). The aircraft states were lateral velocity v (m/s), roll rate p (rad/s), yaw rate r (rad/s), roll attitude ϕ (rad). Additionally, actuator lag states T_{lat} and T_{yaw} were applied to the lateral and yaw inputs, respectively. This improves the accuracy of the fit by modeling the first order characteristic of the motor response as also confirmed in Ref. [3, 13]. This effectively multiplies the lateral responses by a first order lag, for example:

$$\frac{p}{\delta_{lat}} = \left(\frac{p}{\delta'_{lat}} \right) \left(\frac{\omega_{lag}}{s + \omega_{lag}} \right) \quad (2)$$

where p/δ'_{lat} is the response with instantaneous thrust. The yaw response is a combination of differential motor torques on alternating rotors, which produces a

System Identification Software

CIFER[®] (Comprehensive Identification from Frequency Responses) is an integrated software, used for system identification [3]. CIFER[®] was utilized for the work herein because it is a well-established frequency domain method, which is well suited for unstable dynamics and high vibration due to the six rotors of the hexacopter. The software was used to extract non-parametric control-to-vehicle frequency responses from flight data, develop flight accurate state-space models, and perform time-domain verification on these models.

LATERAL-DIRECTIONAL MODEL IDENTIFICATION AT HOVER

Automated frequency sweeps were performed on the University of Portland hexacopter at the hovering flight condition. The resulting data were used to determine a high quality, flight accurate state-space model. On-axis derivatives were identified from the flight test data of the hexacopter, using the model structure shown in Eqn. 1. All axes in this model were decoupled due to the decoupled response of the aircraft, which results from the counter-rotating and symmetric propeller configuration. The lateral-directional state-space model structure is given by Eqn. 1:

lead-lag motor dynamic. This is implemented in the model by including a lagged control derivative $N_{\delta_{yaw}}$ and lead control derivative $N'_{\delta_{yaw}}$:

$$\frac{r}{\delta_{yaw}} = \left(\frac{r}{\delta'_{yaw}} \right) \left(\frac{s + \omega_{lead}}{s + \omega_{lag}} \right) = \left(\frac{N'_{\delta_{yaw}}}{s - N_r} \right) \left(\frac{s + \omega_{lead}}{s + \omega_{lag}} \right) \quad (3)$$

where the lead frequency can be calculated from the identified parameters as:

$$\omega_{lead} = \omega_{lag} \left(1 + \frac{N_{\delta_{yaw}}}{N'_{\delta_{yaw}}} \right) \quad (4)$$

Output Equations

In system identification, output equations are needed to map the measured frequency response outputs to the model states. The outputs (y) used in the system

identification for the lateral-directional model were [4]:

$$y = [p \ r \ a_{y_m} \ \dot{v}_m] \quad (5)$$

The angular rate gyro sensors and the lateral accelerometers are built into the Pixhawk. The lateral velocity rate is reconstructed (at hover $u_o, w_o, \theta_o = 0$):

$$\dot{v} = a_y + g\phi \quad (6)$$

When using the equations of motion, the assumption is that the center of mass is where the data measurement device is located. If the measurement device cannot be placed directly at the center of mass, an offset term is used to account for the displacement between the center of mass and the measurement device. For the UP hexacopter, an offset was only present in the vertical direction, which affects the lateral acceleration as measured:

$$a_{y_m} = a_y - z_a \dot{p} \quad (7)$$

z_a is the z-body axis offset distance from the center of mass to the sensor. The velocity rate was reconstructed at the sensor, using the accelerations that are measured at an offset from the center of gravity:

$$\begin{aligned} \dot{v}_m &= a_{y_m} + g\phi \\ &= a_y - z_a \dot{p} + g\phi = \dot{v} - z_a \dot{p} \end{aligned} \quad (8)$$

The offset of the accelerometer, which is housed in the Pixhawk, was calculated as $z_a = 0.03$ m. The final output matrix, which models the measured output parameters as function of the states, is then:

$$\begin{bmatrix} p \\ r \\ a_{y_m} \\ \dot{v}_m \end{bmatrix} = \begin{bmatrix} 0 & 1 & 0 & 0 \\ 0 & 0 & 1 & 0 \\ 0 & 0 & 0 & -9.81 \\ 0 & 0 & 0 & 0 \end{bmatrix} \begin{bmatrix} v \\ p \\ r \\ \phi \end{bmatrix} + \begin{bmatrix} 0 & 0 & 0 & 0 \\ 0 & 0 & 0 & 0 \\ 1 & -0.03 & 0 & 0 \\ 1 & -0.03 & 0 & 0 \end{bmatrix} \begin{bmatrix} \dot{v} \\ \dot{p} \\ \dot{r} \\ \dot{\phi} \end{bmatrix} \quad (9)$$

Speed Damping Derivative Y_v

In system identification of helicopters, the speed damping parameter Y_v (and similarly, X_u) is often found to be insensitive in the model structure identification [4, 14]. However, this term primarily captures the increase in drag as a function of speed, so it must have a nonzero negative value. Similarly, these speed derivatives are also insensitive for the hexacopter. This derivative can be accurately

identified for a helicopter based on a simple low frequency approximation [4, 14], which also works well on a hovering hexacopter:

$$\frac{\dot{v}}{p} = \frac{g}{(s - Y_v)} \quad (10)$$

Where \dot{v}/p is calculated via frequency response arithmetic using the reconstructed \dot{v} with center of mass correction:

$$\frac{\dot{v}}{p} = \frac{\dot{v}_m}{\delta_{lat}} + z_a \left(s \frac{p}{\delta_{lat}} \right) \quad (11)$$

The model fit was performed by using a transfer function fitting routine (NAVFIT, CIFER[®]) as shown in Figure 3, where $Y_v = -0.221 \text{ s}^{-1}$ is identified.

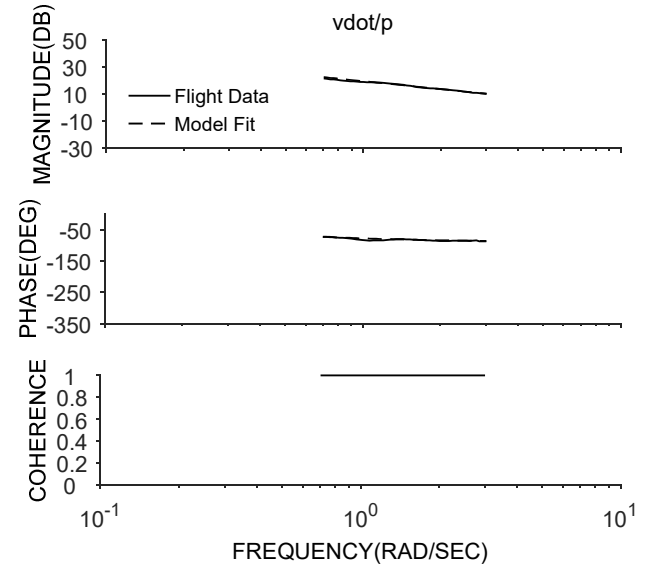


Figure 3. Transfer Function Fit of \dot{v}/p , with $Y_v = -0.221 \text{ s}^{-1}$.

Identified Hover State-Space Model: Lateral-Directional

The identified model parameters, corresponding to the model structure in Eqn. 1, are shown in Table 1. An ideal model should have an average cost $J_{ave} < 100$, Cramer-Rao bounds $CR < 20\%$ and insensitivities $I < 10\%$. A model structure determination process was used, following the guidance in Ref. [4], where parameters were dropped or fixed at an estimated value (as in the case of Y_v) if insensitivities were $I > 10\%$ and Cramer-Rao bounds were $CR > 20\%$. If the average cost jumped significantly after dropping a term, then the parameters were reintroduced back into

the model structure even with less than desired theoretical accuracy. The angular damping derivative L_p is seen to be dropped from the model structure as unimportant for the hovering dynamics, where the large dihedral derivative L_v dominates the roll response. This is consistent with other hover model identification for multicopters [2, 3]. For the identified hexacopter model, all Cramer-Rao bounds and Insensitivity guidelines were achieved, as shown in *Table 1*, indicating very good theoretical accuracy. The frequency response costs are shown in *Table 2*. The resulting lateral-directional model had an average cost of $J_{ave} = 54.2$, indicating excellent predictive accuracy in the frequency domain. It should be noted that many of the parameters are tied to the longitudinal-heave model structure, which constrains the problem via the symmetry of the dynamics for pitch and roll observed at hover, further improving theoretical accuracy, but increasing the model cost slightly. *Figure 4* and *Figure 5* show frequency response comparisons for the identified state space model as compared with the flight data. Each individual frequency response shows excellent agreement, over a wide frequency range, between the identified model and flight data, confirming the low individual cost functions in *Table 2*.

The eigenvalues (λ_i) of the identified model are located in *Table 3*. The first eigenvalue is the yaw mode, which is an integrator ($s = 0$) because the yaw damping of the hexacopter is negligible, $N_r = 0$. Eigenvalues two and three are the unstable oscillatory mode. The fourth eigenvalue is the stable aperiodic roll mode. Eigenvalues 2-4 make up the unstable hovering cubic, which is characteristic of any hovering vehicle [4]. The fifth and sixth eigenvalues are the motor/rotor lag mode ($-\omega_{lag}$).

Time Domain Verification: Lateral-Directional

The identified lateral-directional model was verified in the time domain by comparing the flight test data from a doublet maneuver with the model extracted from the frequency sweep data. The model very accurately predicts the flight data collected from roll and yaw doublets, shown in *Figure 6* and *Figure 7*, with nearly imperceptible difference between the model and flight data. For a full scale vehicle, the verification cost should be $J_{RMS} < 1 - 2$ and $TIC < 0.35$ [3]. For small scale UAS, the verify cost should be Froude scaled to account for the large response magnitude achieved by

multirotor vehicles, as exemplified by the roll rate in *Figure 6*. An adjustment factor was based on Froude scaling [5] as determined by comparing the hub-to-hub distance of the multirotor relative to the rotor diameter of the UH-60, a representative full-scale configuration, resulting in $N = 1/29.8$. The raw roll-axis cost was $J_{RMS} = 1.57$ with $J_{Froude} = J_{RMS}\sqrt{N} = 0.288$, and normalized cost $TIC = 0.043$ (~4% error). The yaw-axis Froude-scaled verify cost was $J_{Froude} = 0.6380$ and $TIC = 0.054$ (~5% error). These time-domain Froude-scaled cost function results, in combination with *Figure 6* and *Figure 7*, confirm the excellent predictive accuracy of the identified lateral-directional model at hover.

Table 1. Lateral-Directional Model Parameters at Hover.

Parameter	Value	Cramer-Rao (%)	Insensitivity (%)
Y_v (1/s)	-0.221	-	-
L_v ($\frac{\text{rad/s}}{\text{m}}$)	-4.01	5.21	1.88
L_p (1/s)	0	-	-
N_r (1/s)	0	-	-
$L_{\delta_{lat}}$ ($\frac{\text{rad/s}^2}{\%/100}$)	145	2.93	2.11
$N_{\delta_{ped}}$ ($\frac{\text{rad/s}^2}{\%/100}$)	-22.5	9.68	1.51
$N_{\delta_{ped}}$ ($\frac{\text{rad/s}^2}{\%/100}$)	34.1	6.03	0.914
ω_{lag} (rad/s)	15	5.16	2.07
τ_{lat} (s)	0.02	-	-
τ_{ped} (s)	0.02	-	-

Table 2. Lateral-Directional Frequency Response Costs at Hover.

Frequency Response	Cost
a_y/δ_{lat}	59.7
p/δ_{lat}	52.0
\dot{v}/δ_{lat}	79.9
r/δ_{ped}	25.1

Average Cost: $J_{ave} = 54.2$

Table 3. Lateral-Directional Model Eigenvalues at Hover.

Eigenvalue Number, λ_i	Mode	Real (rad/s)	Imaginary (rad/s)	Damping Ratio	Natural Frequency (rad/s)
1	Yaw	0	0	-	-
2	Roll Oscillatory	1.63	2.93	- 0.485	3.35
3	Roll Oscillatory	1.63	- 2.93	- 0.485	3.35
4	Roll Mode	-3.46	0	-	-
5	Motor Lag	-15	0	-	-
6	Motor Lag	-15	0	-	-

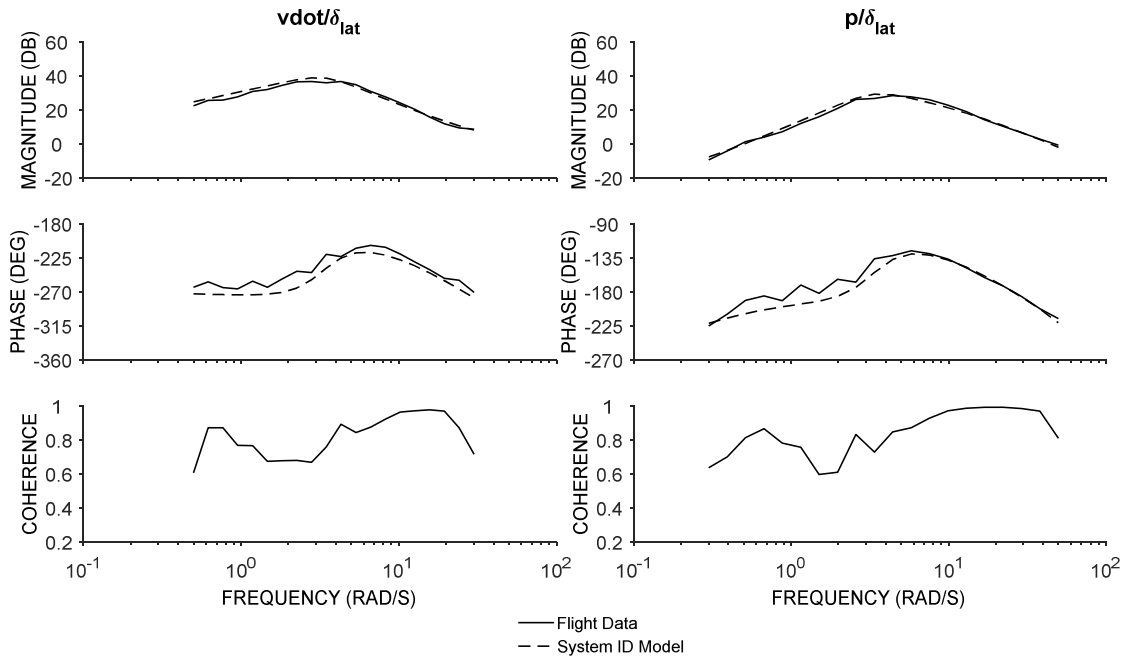


Figure 4. Lateral Body Velocity Rate and Roll Rate Models versus Flight Data.

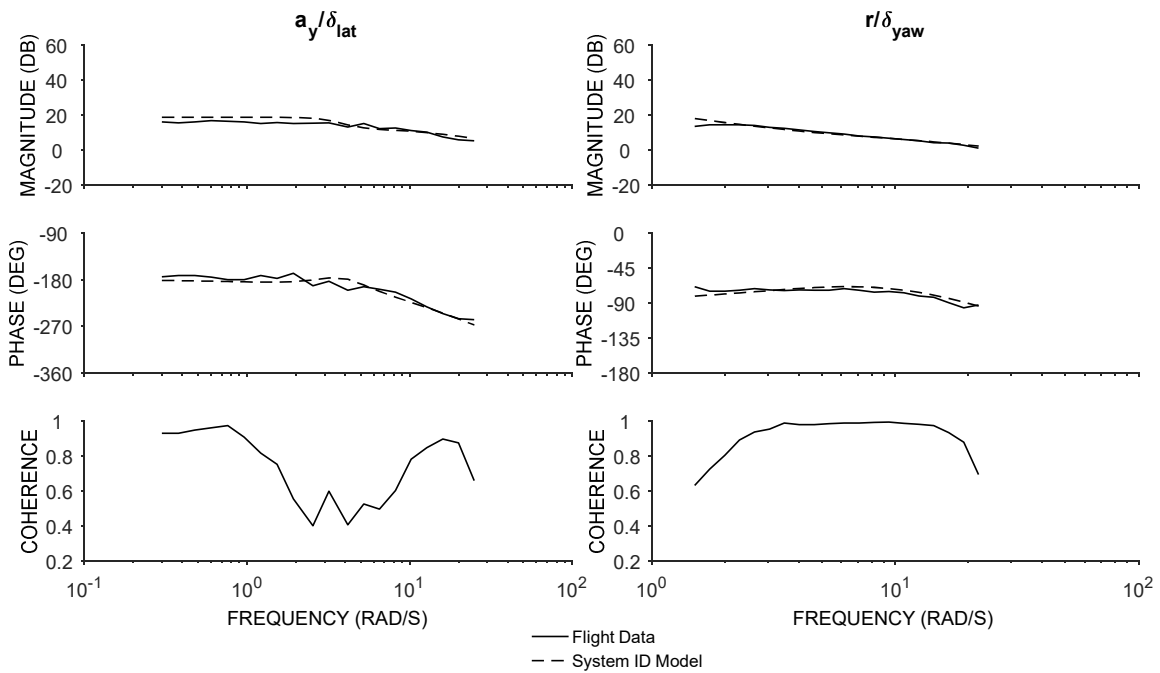


Figure 5. Lateral Body-Axis Accelerometer and Yaw Rate Models versus Flight Data.

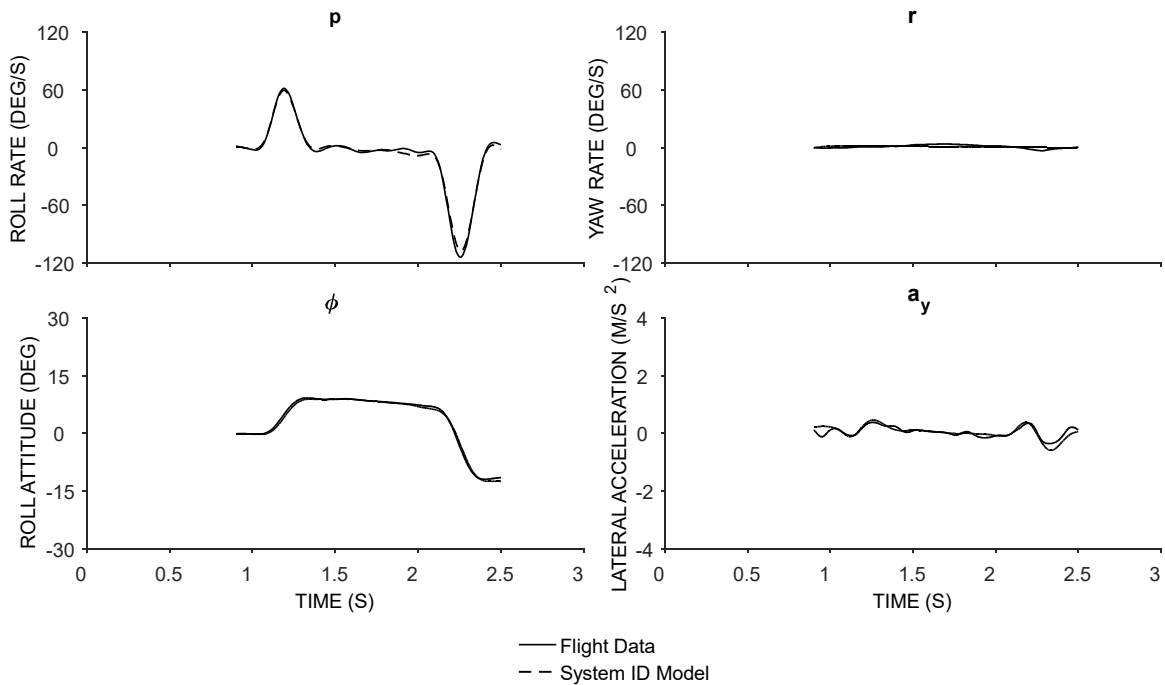


Figure 6. Lateral-Input Time Domain Verification at Hover.

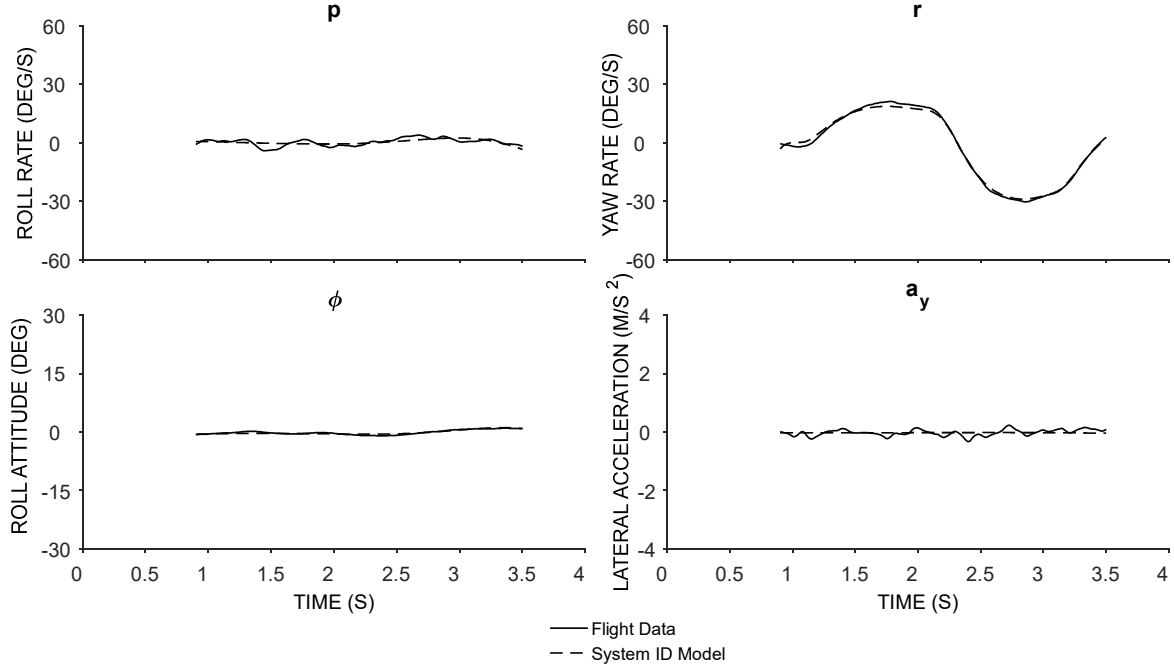


Figure 7. Yaw-Input Time Domain Verification at Hover.

LONGITUDINAL-HEAVE MODEL IDENTIFICATION AT HOVER

A similar process to the determination of the lateral-directional dynamics was employed to identify a longitudinal-heave state-space model. Longitudinal and heave axis frequency sweeps were performed on the University of Portland hexacopter. The resulting data were used to determine a high quality, flight accurate state-space model of the longitudinal-heave dynamics at hover.

Model Structure

Similar to the lateral-directional model, only on-axis derivatives were identified from the flight test data of the hexacopter, using the model structure shown in Eqn. 12. The lateral and longitudinal models were simultaneously identified, so that parameters constrained by symmetry of the physics could be constrained in the model identification (such as $X_u = Y_v$). This model was decoupled due to the decoupled response of the hexacopter resulting from the counter-rotating propeller configuration. The model structure was:

$$\begin{bmatrix} \dot{u} \\ \dot{w} \\ \dot{q} \\ \dot{\theta} \\ \dot{T}_{lon} \\ \dot{T}_{thr} \end{bmatrix} = \begin{bmatrix} X_u & 0 & X_q & -g & 0 & 0 \\ 0 & Z_w & 0 & 0 & 0 & Z_{\delta_{thr}} \\ M_u & 0 & M_q & 0 & M_{\delta_{lon}} & 0 \\ 0 & 0 & 1 & 0 & 0 & 0 \\ 0 & 0 & 0 & 0 & -\omega_{lag} & 0 \\ 0 & 0 & 0 & 0 & 0 & -\omega_{lag} \end{bmatrix} \begin{bmatrix} u \\ w \\ q \\ \theta \\ T_{lon} \\ T_{thr} \end{bmatrix} + \begin{bmatrix} 0 & 0 \\ 0 & 0 \\ 0 & 0 \\ 0 & 0 \\ \omega_{lag} & 0 \\ 0 & \omega_{lag} \end{bmatrix} \begin{bmatrix} \delta_{lon}(t - \tau) \\ \delta_{thr}(t - \tau) \end{bmatrix} \quad (12)$$

$$\frac{q}{\delta_{lon}} = \left(\frac{q}{\delta'_{lon}} \right) \left(\frac{\omega_{lag}}{s + \omega_{lag}} \right) \quad (13)$$

$$\frac{w}{\delta_{thr}} = \left(\frac{w}{\delta'_{thr}} \right) \left(\frac{\omega_{lag}}{s + \omega_{lag}} \right) \quad (14)$$

The inputs to the model are the longitudinal control-axis input δ_{lon} and the thrust control-axis input δ_{thr} , both measured just upstream of the mixer (in normalized units, %/100). The aircraft states were longitudinal velocity u (m/s), vertical velocity w (m/s), pitch rate q , (rad/s), and pitch attitude θ (rad). Two motor lag states T_{lon} and T_{thr} were also introduced in the longitudinal-heave model, as in the lateral-directional model, in order to improve the high frequency fit of the pitch and heave responses. This improves the accuracy of the fit by modeling the first order characteristic of the motor responses [3, 13] that affects the control response as shown in *Eqns. (13-14)*.

Output Equations

The outputs used in the system identification for the longitudinal-heave model were:

$$y = [a_{x_m} \dot{u}_m q \theta a_{z_m}]^T$$

The output equations map the model states and measured outputs. Just as in the lateral-directional models, a vertical cg offset $z_a = 0.03$ m was included in the accelerometer output (a_{x_m}) and body velocity rate (\dot{u}_m) outputs:

$$\begin{bmatrix} a_{x_m} \\ \dot{u}_m \\ q \\ \theta \\ a_{z_m} \end{bmatrix} = \begin{bmatrix} 0 & 0 & 0 & 9.81 \\ 0 & 0 & 0 & 0 \\ 0 & 0 & 1 & 0 \\ 0 & 0 & 0 & 1 \\ 0 & 0 & 0 & 0 \end{bmatrix} \begin{bmatrix} u \\ w \\ q \\ \theta \end{bmatrix} + \begin{bmatrix} 1 & 0 & 0.03 & 0 \\ 1 & 0 & 0.03 & 0 \\ 0 & 0 & 0 & 0 \\ 0 & 0 & 0 & 0 \\ 0 & 1 & 0 & 0 \end{bmatrix} \begin{bmatrix} \dot{u} \\ \dot{w} \\ \dot{q} \\ \dot{\theta} \end{bmatrix} \quad (15)$$

Speed Damping Derivative X_u

The speed derivative X_u was insensitive in the system identification optimization cost. To maintain symmetry with the roll-axis dynamics, the value of X_u was selected as $X_u = Y_v = -0.221$.

$$\frac{\dot{u}}{q} = \frac{-g}{(s-X_u)} \quad (16)$$

The validity of this assumption was verified in NAVFIT, by evaluating the fit of \dot{u}/q using *Eqn. (16)* with $X_u = -0.221, s^{-1}$. The pitch axis had a similarly excellent fit as that shown for the lateral axis in *Figure 3*.

Identified Hover State-Space Model: Longitudinal-Heave

The Cramer-Rao bounds, insensitivities and the parameters identified are located in *Table 4*. The model has Cramer-Rao and Insensitivities well within the guidelines of 20% and 10%, respectively, for all except the Z_w derivative which is just outside theoretical accuracy guidelines. Many of the pitch derivatives are constrained to the roll-axis symmetric counterpart, resulting in improved theoretical accuracy. The longitudinal and heave frequency response cost functions are located in *Table 5*, indicating good accuracy of the identified model ($J < 100$ is good, $J < 50$ is excellent). *Figure 8* and *Figure 9* show frequency responses for the identified state-space model as compared with the flight data. Each individual frequency response shows good agreement, over a wide frequency range, between the identified model and flight data. The resulting longitudinal-heave model had an excellent average cost of $J_{ave} = 52.2$.

Table 4. Longitudinal-Heave Model Parameters at Hover.

Parameter	Value	Cramer-Rao (%)	Insensitivities (%)
X_u (1/s)	-0.221	-	-
X_q ($\frac{m/s}{rad}$)	0	-	-
Z_w (1/s)	-0.338	21.1	10.3
M_u ($\frac{rad/s}{m}$)	4.01	5.21	1.88
M_q (1/s)	0	-	-
$X_{\delta_{lon}}$ ($\frac{m/s^2}{\%/100}$)	0	-	-
$M_{\delta_{lon}}$ ($\frac{rad/s^2}{\%/100}$)	165	3.78	1.21
$Z_{\delta_{thr}}$ ($\frac{m/s^2}{\%/100}$)	-39.4	2.29	1.35
ω_{lag} (rad/s)	15	5.16	2.07
τ (s)	0.02	-	-

Table 5. Longitudinal-Heave Frequency Response Costs.

Frequency Response	Cost
\dot{u}/δ_{lon}	86.2
q/δ_{lon}	58.9
a_x/δ_{lon}	50.4
a_z/δ_{thr}	13.1

Average Cost: $J_{ave} = 52.2$

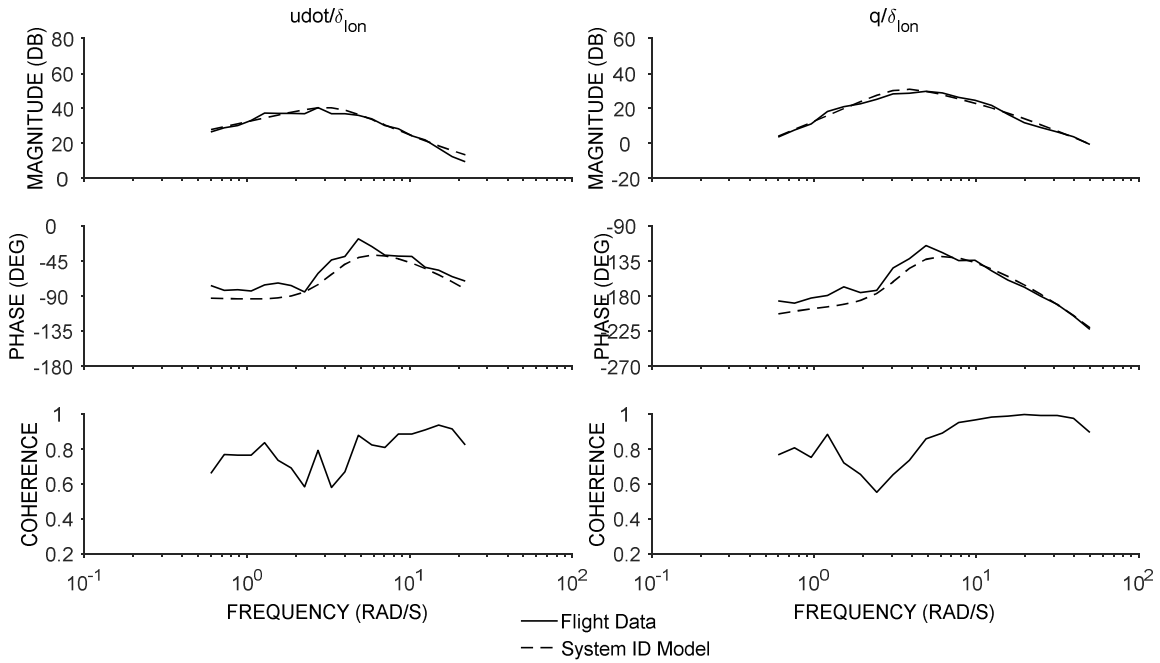


Figure 8. Longitudinal Body Velocity Rate and Pitch Rate Models versus Flight Data.

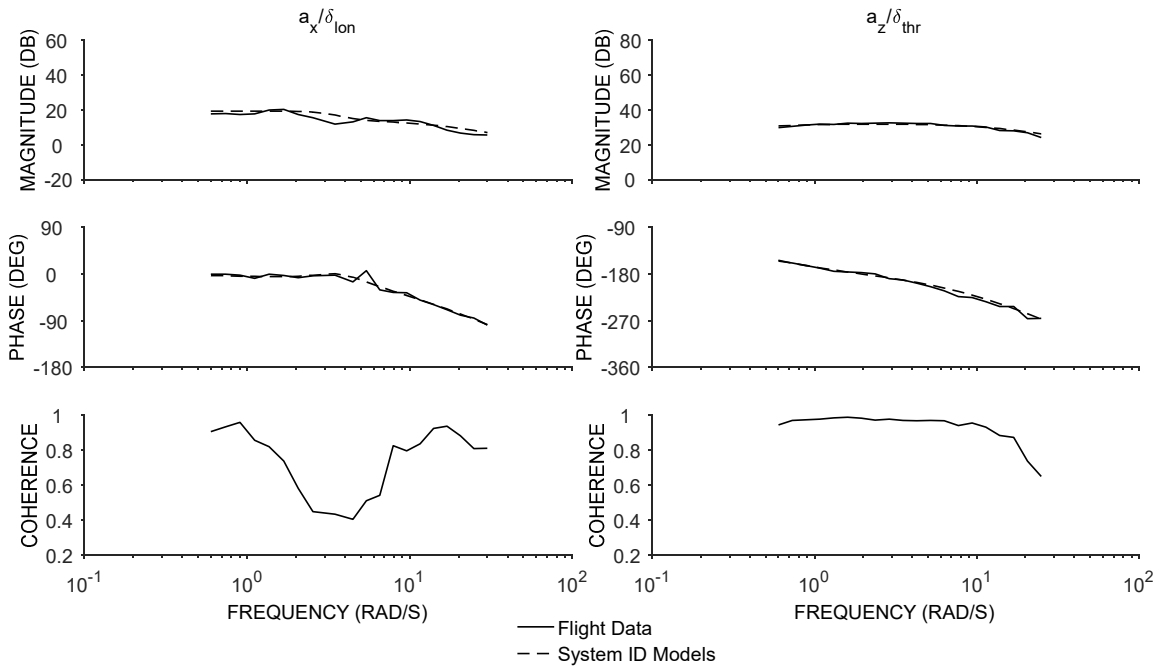


Figure 9. Longitudinal Body Acceleration and Heave Body Acceleration Models versus Flight Data.

Eigenvalues

The eigenvalues of the model λ_i are located in Table 6. The first eigenvalue is the heave mode with frequency $\lambda_1 = -Z_w$. Eigenvalues two and three are the unstable oscillatory mode. The fourth eigenvalue is the pitch mode. Eigenvalues 2-4 make up the unstable hovering cubic, which is characteristic of any hovering vehicle. The fifth and sixth eigenvalues are the motor lag modes ($-\omega_{lag}$). The longitudinal eigenvalues ($\lambda_2 - \lambda_5$) match the lateral-directional eigenvalues ($\lambda_2 - \lambda_5$), due to the enforced model symmetry.

Time Domain Verification: Longitudinal-Heave

As in the lateral-directional model, the longitudinal-heave model was verified in the time domain by

comparing the flight test data from a doublet maneuver to the model extracted from the frequency sweep data, and assessed using the Froude-scaled cost J_{Froude} . The model accurately predicts the flight data collected from the doublet, shown in *Figure 10* for a longitudinal input. The corresponding Froude scaled cost is $J_{Froude} = J\sqrt{1/N} = 0.278$ and normalized cost $TIC = 0.041$ (~4%), which are well below the recommendations ($J_{Froude} < 1 - 2$ and $TIC < 0.35$). The heave-axis (throttle-input) time domain prediction is also very good as shown in *Figure 11*. The Froude scaled verify cost was $J_{Froude} = 0.36$ and TIC was 0.09. These time-domain cost function results confirm the good predictive accuracy of the identified model.

Table 6. Longitudinal-Heave Model Eigenvalues at Hover.

Eigenvalue Number, λ_i	Mode	Real (rad/s)	Imaginary (rad/s)	Damping Ratio	Natural Frequency (rad/s)
1	Heave	-0.338	-	-	-
2	Pitch Oscillatory	1.63	2.93	-0.485	3.35
3	Pitch Oscillatory	1.63	-2.93	-0.485	3.35
4	Pitch Mode	-3.46	-	-	-
5	Motor Lag	-15	-	-	-
6	Motor Lag	-15	-	-	-

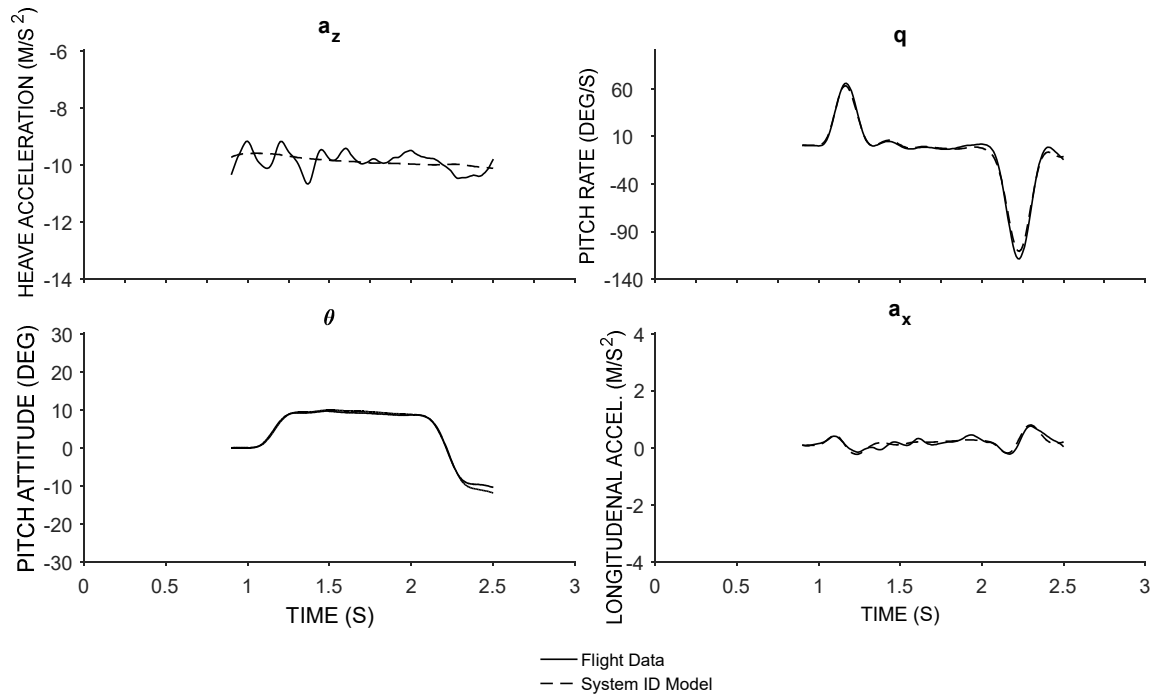


Figure 10. Pitch-Input Time Domain Verification at Hover.

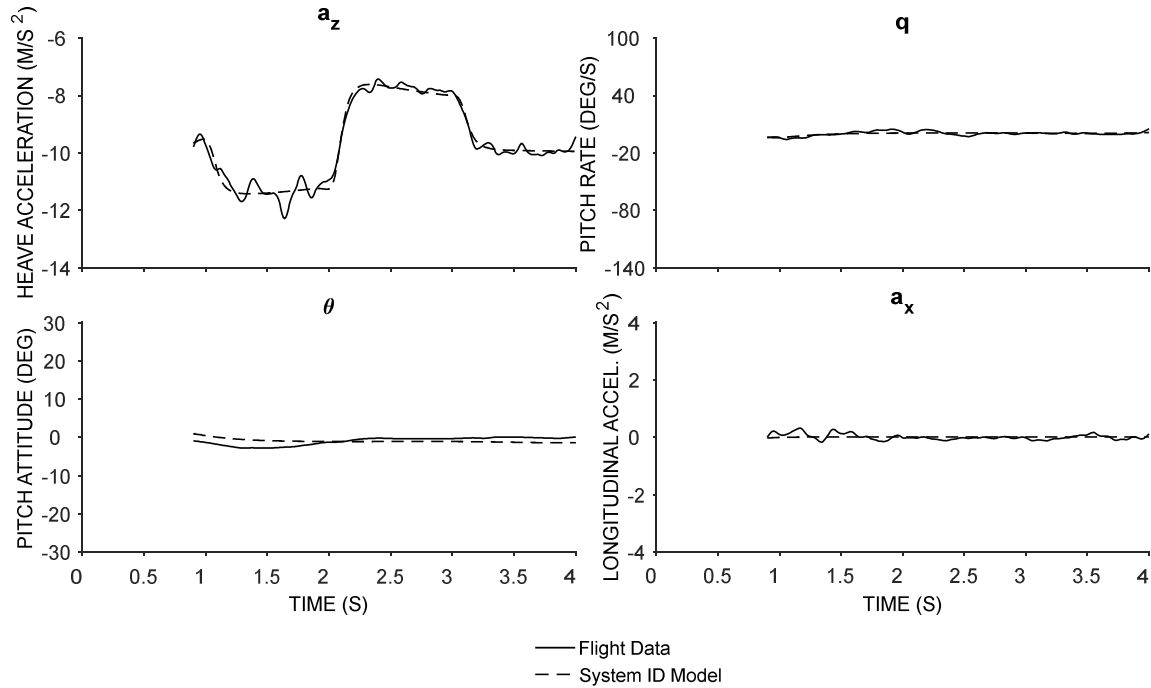


Figure 11. Throttle-Input Time Domain Verification at Hover.

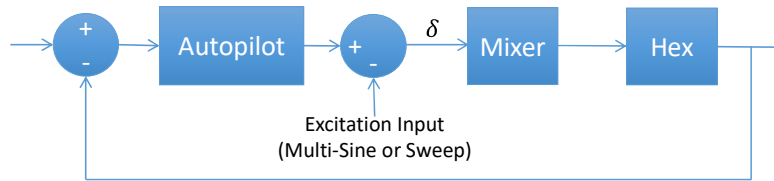


Figure 12. Block Diagram of Control Input.

TESTING GUIDANCE: SYSTEM ID OF MULTIROTOR AERIAL VEHICLES

A parametric variation of frequency sweep amplitudes was performed in all axes (roll, yaw, pitch and heave) in order to provide guidance on frequency sweep amplitude for small scale multirotor UAS. The frequency sweeps were input at the mixer as shown in *Figure 12* and amplitudes of the sweep was varied as appropriate for the control axis. Sweeps were performed in the “stabilize” mode of the Arducopter. The resulting response magnitudes were recorded, and are shown in *Table 7*, characterizing the low, medium and high amplitude cases in each axis.

State-space models were identified from each set of frequency sweep data. The criteria for selecting the best models were based on frequency domain cost values, Cramer-Rao Bounds and verify costs. The costs were averaged for each control axis, as opposed

to combined longitudinal-heave and lateral-directional costs shown earlier in the paper. The low amplitude sweeps provided the best models across the board. It should be noted that these low amplitude sweeps were used in the results that are presented in the previous sections of the paper. Based on the results of *Table 7*, it is recommended that the longitudinal and lateral sweeps produce approximately ± 125 deg/s of pitch and roll rate for best results. When Froude scaled, this is equivalent to ± 23 deg/s in full-scale angular rates. The guidance for full scale frequency sweeps in Ref. [3] is to achieve angular rates on the order of ± 10 deg/s. The reason for the larger scaled amplitudes on the multirotor vehicle may be due to reduced signal-to-noise ratios from the small-scale sensor and the larger influence of any turbulence on the response. Based on *Table 7*, the yaw-axis sweep is recommended to produce ± 30 deg/s of yaw-rate response. This Froude scales to approximately 6 deg/s of full scale response, which is similar to the full scale

recommendation. However, it should be noted that the yaw response was less sensitive to amplitude and had similar characteristics for all amplitude sweeps – this may be due to the fact that the yaw response stays at the hover condition regardless of the amplitude of the sweep and so is more linear. The heave axis results produced the best result with +/- 4 m/s² of response,

which is still 4 m/s² of acceleration when Froude scaled, and is about twice the accelerations used in full scale sweeps. A general recommendation would be that the Froude scaled (to full scale) frequency sweep amplitude should be roughly twice the recommendations found in [4].

Table 7. Variation in Amplitude Effects on System Identification Results at Hover.

Sweep Amplitude	Metric	Roll Axis	Yaw Axis	Pitch Axis	Heave Axis
Low	Max On-Axis Response Amplitude	+/- 125 deg/s +/- 10 deg	+/- 30 deg/s +/- 20 deg	+/- 125 deg/s +/- 10 deg	+/- 4 m/s ² +/- 1.3 m/s
	Average Model Cost (Frequency Domain)	63.9	25.1	65.2	13.1
	Average Cramer Rao (%)	4.43	7.85	4.72	11.7
	Verification TIC Cost	0.04	0.05	0.04	0.09
Medium	Max On-Axis Response Amplitude	+/- 190 deg/s +/- 20 deg	+/- 85 deg/s +/- 25 deg	+/- 140 deg/s +/- 15 deg	+/- 5 m/s ² +/- 4 m/s
	Average Model Cost (Frequency Domain)	82.9	29.0	90.4	28.3
	Average Cramer Rao (%)	17.2	24.9	6.07	6.83
	Verification Cost (Time Domain)	0.09	0.09	0.11	0.17
High	Max On-Axis Response Amplitude	+/- 230 deg/s +/- 30 deg	+/- 95 deg/s +/- 45 deg	+/- 195 deg/s +/- 20 deg	+/- 8 m/s ² +/- 4 m/s
	Average Model Cost (Frequency Domain)	166	35.5	105.8	32.4
	Average Cramer Rao (%)	5.57	11.2	6.16	5.66
	Verification Cost (Time Domain)	0.14	0.15	0.14	0.22

MULTI-SINE INPUT EXCITATION FOR SYSTEM IDENTIFICATION OF MULTROTOR VEHICLES

Another frequently used maneuver for system identification flight testing is the multi-sine input [6, 7]. Multi-sine inputs add together sine waves at discrete frequencies to create a single input signal that excites the desired frequency range. The equations below describe the input to the aircraft control surfaces that is a set of summed harmonic sinusoids with individual phase lags [6].

$$u_j = \sum_k^{1,2,3,\dots,M} \cos\left(\frac{2\pi kt}{T} + \phi_k\right) \quad (17)$$

$$\phi_k = \frac{\pi n^2}{N} \quad (18)$$

The input u_j is applied to the j^{th} control surface, and the total number of harmonically-related frequencies (M) is the maximum frequency range desired. T is the time length of the excitation and ϕ_k are the phase angles for each given frequency k . The multi-sine inputs are orthogonal and can be applied across all control inputs

simultaneously. However, it should be noted that in the case where the model structure is not decoupled and the control system is engaged, the inputs will be fully correlated [15]. For a fully decoupled model structure, such as the hover condition presented herein with inputs at the mixer, it is possible to use simultaneous inputs. However, only a single axis input was used to provide better frequency resolution and better direct comparison with the frequency sweep inputs.

Resulting frequency responses using two concatenated records from multi-sine inputs versus two concatenated records from Frequency Sweep inputs are compared in *Figure 13* for pitch axis system identification (q/δ_{lon}). The multi-sine is only plotted at the discrete input excitation frequencies. Every effort was made to ensure that the multi-sine and the frequency sweep had similar input frequency content and amplitude to ensure a fair comparison of the two maneuvers. The power spectral density signals across the frequency range of interest are shown in the first column of *Figure 13*. The power spectral density for the excitation signal, inserted upstream of the mixer, as shown in *Figure 12*, was selected to be similar for

the multi-sine and frequency sweep inputs. As shown by *Figure 13*, the frequency sweep signal has more content at lower frequency and less at higher frequency, due to its exponential frequency progression, whereas the multi-sine is designed to provide a flat spectrum. Still, this averages out to about the same spectral content. The total input signal is the sum of the excitation signal and the control system input (labeled as δ in *Figure 12*). For this signal, *Figure 13* indicates that the spectral content is slightly higher for the multi-sine input, resulting from the control system response to the multi-sine input. The output power spectral density of the pitch rate,

indicates similar response amplitudes, but again slightly higher for the multi-sine. Despite the lower total input to output amplitude of the frequency sweep, the frequency sweep still has an overall higher coherence compared to the pitch Multi-Sine input as shown in *Figure 13*, especially in the 7-15 rad/s range. Coherence represents the accuracy, quality and linearity of the frequency response. A higher coherence means the data is of better quality. These results indicate a preference for the frequency sweep in this application.

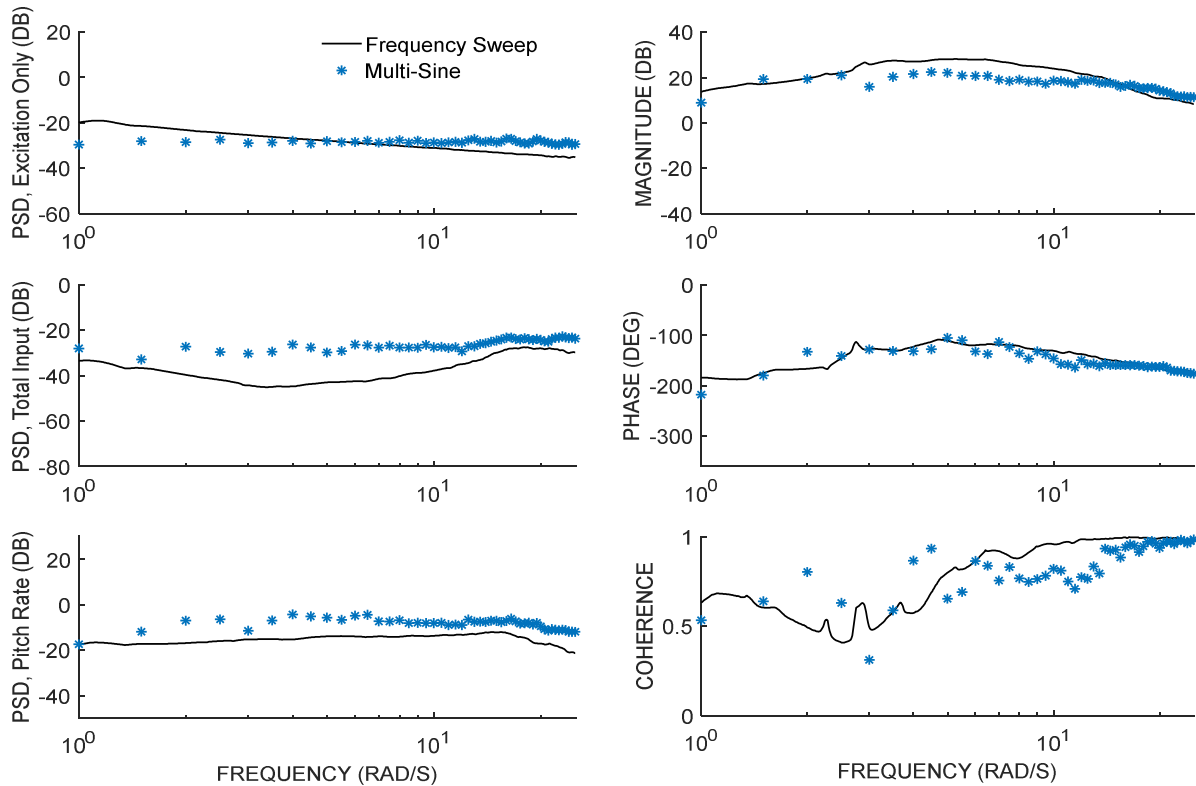


Figure 13. Spectral Data and Frequency Responses for q/δ_{lon} Using Multi-Sine and Frequency Sweep Inputs.

DYNAMIC RESPONSE SCALING FOR MULTIROTOR VEHICLES

It would be useful to utilize an identified state-space model of a one multirotor vehicle and extrapolate the dynamics to larger/smaller scale. This is especially important when considering control system design and handling qualities metrics, for which it is important to be able to scale as opposed to developing new metrics for every possible vehicle size class. To address this

area of interest, a comparison of the identified dynamics of the University of Portland (UP) hexacopter, shown herein, and the larger Aviation Development Directorate (ADD) hexacopter [16] was performed. The two vehicle specifications are compared in *Table 8*.

The Froude number relates inertial force to gravity force via a characteristic length. Scaling rotor dynamics based on the Froude number is a common

similarity requirement for rotorcraft models [5, 17]. Froude scale was shown to work well for scaling fixed-wing aircraft dynamic modes, as observed by Sanders [12]. There is some prior evidence in the literature that the characteristic length used in Froude scaling for multirotor aircraft should be based on the hub-to-hub distance D_{hub} as opposed to disk diameter that is commonly used for a single rotor helicopter [18, 11]. Using D_{hub} as the characteristic length gives:

$$N = N_{D_{hub}} = \frac{D_{hubUP}}{D_{hubADD}} = \frac{55.9}{127} = \frac{1}{2.27} = 0.44 \quad (19)$$

This indicates that the UP hexacopter is $\frac{1}{2.27}$ scale, or nearly half scale relative to the ADD hexacopter. The scaling results for the stability derivatives are shown in Table 9, against the true ADD hexacopter system identification results. The Froude scaled estimates are within $\pm 11\%$ of the true stability derivatives, with the exception of Z_w . This is likely because Z_w is less accurately known in the identification as shown by the larger Cramer-Rao bound in Table 4. It should be noted that the L_p and M_q derivatives could not be identified for the UP hexacopter at hover and therefore cannot be scaled. These parameters were insensitive, indicating that the angular rate damping does not affect the dynamics in the frequency range of interest for the identification (1-30 rad/s). These parameters are likely present, but very small and therefore not important for a good prediction of the dynamic behavior. Small (or zero) angular rate damping at hover is a common result for multirotor vehicles [2, 3, 13]. A comparison of the associated scaled eigenvalues in Table 10 also shows that all modes are well predicted by Froude scaling based on D_{hub} .

Froude scaling as applied to the control derivatives is shown in Table 11. Scaling based on D_{hub} predicted the control moment derivatives $M_{\delta_{lon}}$, $L_{\delta_{lat}}$, $N_{\delta_{yaw}}$ within 18%. The scaling under-predicts $M_{\delta_{lon}}$, $L_{\delta_{lat}}$ by approximately 17% and 14%, respectively. This may be related to discrepancies in the relative scaled

inertias of the two aircraft. When backing out the Froude number from the inertias, the scale factor is:

$$N_{inertia} = \left(\frac{I_{xUP}}{I_{xADD}} \right)^{\frac{1}{5}} = \left(\frac{I_{yUP}}{I_{yADD}} \right)^{\frac{1}{5}} \approx \left(\frac{I_{zUP}}{I_{zADD}} \right)^{\frac{1}{5}} = 0.56 \quad (20)$$

which is a larger characteristic length than when using the hub-to-hub distance. If the Froude scale were to be based on the rotor diameter, an even larger characteristic length would result:

$$N_{D_{rotor}} = \frac{D_{rotorUP}}{D_{rotorADD}} = 0.713 \quad (21)$$

In an ideal world, the inertia, rotor diameter, mass and other physical properties of the aircraft would all scale consistently. However, these two aircraft were not built to be dynamically similar; they are made of different material and the UP blades are much larger relative to the body than the ADD blades. Despite these scaling imperfections, the frequency response prediction is still surprisingly good, as shown by the Bode plots overlaying the scaled UP hexacopter model and the ADD hexacopter model in Figure 14. This shows that the scaling method is robust, and does not require perfectly scaled models to provide a reasonable prediction of the dynamics. This has important implications for scaling handling qualities requirements and flight control design methods [19], where robust scaling of specifications are needed to fit a variety of vehicles in a similar size class.

As a point of interest, the scaled hexacopter frequency responses when using scaling based on the rotor diameter (Eqn. 21) are also shown in Figure 14. The pitch, roll, and yaw frequency responses clearly indicate that the dynamics modes and control moments of the aircraft are not correctly predicted when the ratio of the rotor diameters is used as the characteristic length. The heave frequency response is less sensitive to the choice of characteristic length, as the thrust control derivative scale factor is 1, and Z_w is small.

Table 8. Scale Comparison for Two Hexacopter UAVs.

	UP Hexacopter	ADD Hexacopter
Hub-to-Hub Distance, D_{hub}	55.9 cm	127 cm
Rotor Diameter, D_{rotor}	25.4 cm	35.6 cm
Mass, m	1.56 kg	7.13 kg
Pitch/Roll Inertia, $I_y = I_x$	0.0266 kg · m ²	0.477 kg · m ²
Yaw Inertia, I_z	0.0489 kg · m ²	0.913 kg · m ²

Table 9. Stability Derivatives Froude Scaling Based on Hub-to-Hub Distance ($N = 0.44$) at Hover.

Stability Derivative	Units	Froude Scaling Factor	UP Hex (56 cm)	Scaled UP Hex (to 127 cm)	True ADD Hex (127 cm)	%Error Scaled versus True
X_u	1/s	\sqrt{N}	-0.221	-0.147	-0.167	11.9 %
M_u	$\frac{\text{rad/s}}{\text{m}}$	$N\sqrt{N}$	4.01	1.17	1.09	7.34 %
M_q	1/s	\sqrt{N}	0	0	-0.523	n/a
Y_v	1/s	\sqrt{N}	-0.221	-0.148	-0.167	11.9 %
L_v	$\frac{\text{rad/s}}{\text{m}}$	$N\sqrt{N}$	-4.01	-1.17	-1.09	-8.8 %
L_p	1/s	\sqrt{N}	0	0	-0.610	n/a
Z_w	1/s	\sqrt{N}	-0.338	-0.224	-0.291	-23 %
N_r	1/s	\sqrt{N}	0	0	0	0 %
ω_{lead}	rad/s	\sqrt{N}	5.41	3.59	3.27	9.80 %
ω_{lag}	rad/s	\sqrt{N}	15	9.95	11.0	-9.95 %

Table 10. Scaled Hover Modes.

Mode	Frequency (rad/s)		Damping	
	Scaled UP Hex	True ADD Hex	Scaled UP Hex	True ADD Hex
<i>Lateral-Directional Dynamics</i>				
<i>Unstable Lateral Oscillatory Mode</i>	2.22	2.08	-0.48	-0.41
<i>Stable Roll Mode</i>	2.3	2.44	n/a (1 st order)	
<i>Yaw Mode</i>	0	0	n/a (1 st order)	
<i>Longitudinal-Heave Dynamics</i>				
<i>Unstable Longitudinal Oscillatory Mode</i>	2.22	2.08	-0.48	-0.41
<i>Stable Pitch Mode</i>	2.3	2.44	n/a (1 st order)	
<i>Stable Heave Mode</i>	0.224	0.291	n/a (1 st order)	
<i>Motor Dynamics</i>				
<i>Stable Motor Lag Modes (×6 motors) Mode</i>	9.95	11.0	n/a (1 st order)	
	Frequency (rad/s)		Damping	

Table 11. Control Derivatives Froude Scaling at Hover.

Stability Derivative	Units	Froude Scaling Factor	UP Hex (56 cm)	Scaled UP Hex (N=0.44)	True ADD Hex (127 cm)	%Error (N=0.44)
$L_{\delta_{lat}}$	$\frac{\text{rad/s}^2}{\% / 100}$	N	145	63.8	77.2	-17.4 %
$M_{\delta_{lon}}$	$\frac{\text{rad/s}^2}{\% / 100}$	N	165	72.7	84.4	-13.9 %
$N'_{\delta_{yaw}}$	$\frac{\text{rad/s}^2}{\% / 100}$	N	34.1	15	13.8	8.7 %
$Z_{\delta_{thr}}$	$\frac{\text{ft/s}^2}{\% / 100}$	1	-39.4	-39.4	-42.4	-7.07 %

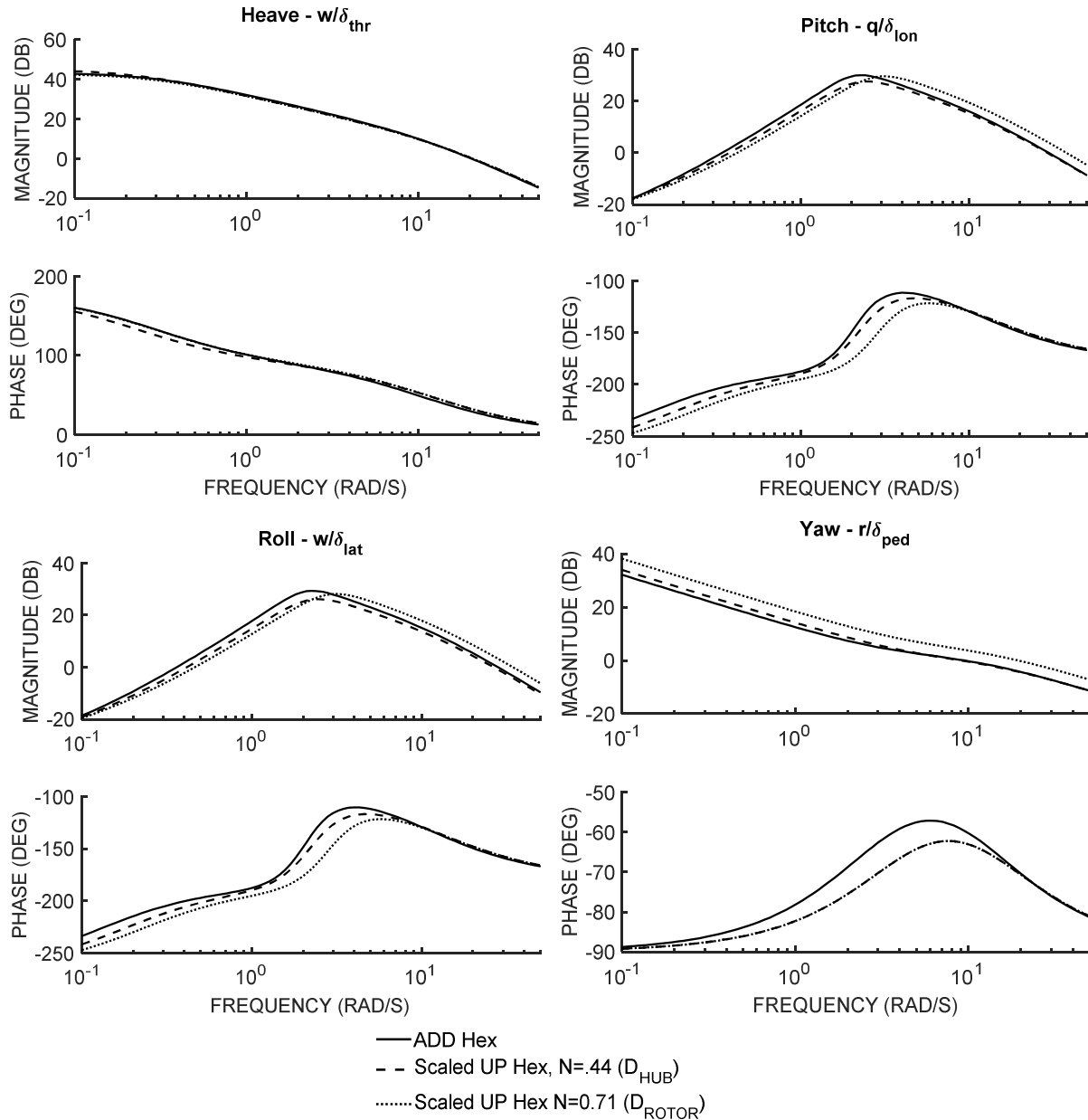


Figure 14. Frequency Responses for Scaled UP Hexacopter versus ADD Hexacopter System ID at Hover.

CONCLUSIONS

Frequency domain system identification was performed in order to extract dynamic models of the University of Portland hexacopter (56 cm, 1.56 kg). Different input excitation techniques were tested to determine recommendations for achieving high quality system identification results on small scale multirotor vehicles. These input excitation techniques included automated frequency sweeps, varying in amplitude, and multi-sine sweeps. Additionally, the concepts of scalability in multirotor vehicles was explored by comparison to system identification

results of a larger hexacopter (127 cm, 7.13 kg). Resulting from this work, several key conclusions can be made:

1. A decoupled state-space model structure, which incorporates motor lag states, well predicts hexacopter dynamics at hover.
2. A parametric variation of frequency sweep amplitudes resulted in the recommendation that the output response angular rates should be approximately ± 125 deg/s for pitch and roll for a small-scale (56 cm) hexacopter. This is equivalent

to ± 23 deg/s in full-scale angular rates (Froude scaled relative to the UH-60), twice the recommended amplitude for full-scale frequency sweeps (10-15 deg/s).

3. The frequency sweep input method resulted in improved coherence and associated frequency response accuracy for extracted models as compared to the multisine input method, even when conducted such that both result in similar output power spectral densities.
4. Froude scaling, based on hub-to-hub distance, is an effective and robust method for scaling multirotor dynamics. This has important implications for scaling handling qualities, where robust scaling of specifications is needed to set requirements for multirotor vehicles in a range of size classes.

REFERENCES

- [1] ArduPilot, "Mission Planner," 2016. [Online]. Available: ardupilot.org.
- [2] W. Wei, K. Cohen and M. Tischler, "System Identification and Controller Optimization of a Quadrotor UAV," in *Proceedings of the AHS International 71st Annual Forum*, Virginia Beach, Virginia, May 5–7, 2015.
- [3] K. Cheung et. al, "An Overview of the U.S. Army Aviation Development Directorate Quadrotor Guidance, Navigation, and Control Project," in *Proceedings of the AHS International 73rd Annual Forum*, Fort Worth, TX, May 9-11, 2017.
- [4] M. Tischler and R. Remple, *Aircraft and Rotorcraft System Identification: Engineering Methods with Flight Test Examples*, Reston, VA: AIAA Education Series, 2012 .
- [5] B. Mettler, M. Tischler and T. Kanade, "System Identification of Small-Sized Unmanned Helicopter Dynamics," in *Proceedings of the American Helicopter Society 55th Annual Forum* , Montreal, Quebec, Canada, May 25-27, 1999.
- [6] E. Morelli, " Multiple Input Design for Real-Time Parameter Estimation in the Frequency Domain," in *13th IFAC Conference on System Identification*, Rotterdam, The Netherlands, Aug 2003.
- [7] E. Morelli and J. A. Graurer, "Practical Aspects of the Frequency Domain Approach for Aircraft System Identification," in *AIAA Aviation Forum Atmospheric Flight Mechanics Conference*, Atlanta, GA, June 2018.
- [8] M. Berrios, T. Berger, M. Tischler, O. Juhasz and F. Sanders, "Hover Flight Control Design for UAS using Performance-based Disturbance Rejection Requirements," in *Proceedings of the American Helicopter Society International Forum*, Fort Worth, TX, May, 2017.
- [9] M. Cotting, "Applicability of Human Flying Qualities Requirements for UAVs, Finding a Way Forward," in *Proceedings of the AIAA Flight Mechanics Conference and Exhibit*, Chicago, IL., August 2009.
- [10] M. Cotting, "UAV Performance Rating Scale Based on the Cooper-Harper Piloted Rating Scale," in *Proceedings of the Aerospace Sciences Meeting*, Orlando, FL, January 2011.
- [11] C. Ivler, C. Goerzen, J. Wagster and F. C. K. T. M. Sanders, "Control Design for Tacking of Scaled MTE Trajectories on an IRIS+ Quadcopter," in *AHS 74th Annual Forum Proceedings*, Phoenix, AZ, May, 2017.
- [12] D. Klyde, D. Mitchell and N. Alexandrov, "Development of a Process to Define Unmanned Aircraft Systems Handling Qualities," in *AIAA Atmospheric Flight Mechanics Conference*, Kissimmee, Florida, 2018.
- [13] A. Gong, F. Sanders, R. Hess and M. Tischler, "System Identification and Full Flight-Envelope Model Stitching of a Package-Delivery Octocopter," in *Proceedings of the AIAA SciTech Forum*, San Diego, CA, Jan 7-11, 2019.
- [14] C. Ivler and M. Tischler, "Case Studies of System Identification Modeling for Flight Control Design," *Journal of the American Helicopter Society*, vol. 58, no. 1, pp. 1-16, January 2013.
- [15] T. Berger, M. Tischler, M. Knapp and M. Lopez, "Identification of Multi-Input Systems in the Presence of Highly-Correlated Inputs," in *Proceedings of the*

- AIAA Scitech Forum , San Diego, CA, 2019.
- [16] M. Lopez, M. Tischler, O. Juhasz, A. Gong and F. Sanders, "Development of a Reconfigurable Mlticopter Flight Dynamics Model from Flight Data using System Identification," in *Proceedings of teh 8th Biennial Autonomous VTOL Technical Meeting*, Mesa, AZ, 2019.
- [17] G. Hunt, "Similarity Requirements for Aeroelastic Models or Helicopter Rotors," R.A.E., C.P. No 1245, Farnborough, January 1972.
- [18] O. Juhasz, M. Tischler and H. Won, "System Identification and Control Law Optimization Applied to the AeroVironment Quantix Tail-Sitter UAS," in *Proceedings of the American Helicopter Society International 74th Annual Forum* , Pheonix, AZ, May, 2018.
- [19] M. Tischler, T. Berger, C. Ivler, M. Mansur, K. Cheung and J. Y. Soong, Practical Methods for Aircraft and Rotorcraft Flight Control Design: An Optimization-Based Approach, Reston, VA: AIAA, 2017.